Two-Dimensional Inductor-Capacitor Lattice Synthesis

Harish S. Bhat and Braxton Osting

***Abstract*—We consider a general class of two-dimensional passive propagation media, represented as a planar graph where nodes are capacitors connected to a common ground and edges are inductors. Capacitances and inductances are fixed in time but vary in space. Kirchhoff's laws give the time dynamics of voltage and current in the system. By harmonically forcing input nodes and collecting the resulting steady-state signal at output nodes, we obtain a linear, analog device that transforms the inputs to outputs. We pose the lattice synthesis problem: given a linear transformation, find the inductances and capacitances for an inductor-capacitor circuit that can perform this transformation. Formulating this as an optimization problem, we numerically demonstrate its solvability using gradient-based methods. By solving the lattice synthesis problem for various desired transformations, we design several devices that can be used for signal processing and filtering.**

***Index Terms*—lattice synthesis, analog circuit design, device sizing, Kirchhoff's laws, inductor-capacitor lattice**

I. Introduction

We investigate a general class of two-dimensional passive propagation media that can be used for signal processing and filtering. These media consist of two-dimensional (2-D) inductor-capacitor (LC) lattices, an example of which is shown in Fig. 1, with spatially varying inductance and capacitance. The lattice is a natural generalization of the one-dimensional transmission line. The 2-D LC lattice was first explored by Léon Brillouin [1], who showed its equivalence to 2-D mass-spring lattices used to model crystals.

In this paper, the input $f_j e^{2\pi\imath\alpha t}$ is applied to node j on the left boundary of the lattice and the steady-state output $g_j e^{2\pi\imath\alpha t}$ is tapped from node j on the right boundary. The choice of inductance $\mathbf{L}$ and capacitance $\mathbf{C}$ vectors defines a transfer function from the inputs to the outputs. If there are m rows in the lattice, then for a fixed basis in $\mathbb{C}^m$, the transfer function can be represented by an $m \times m$ complex matrix, denoted $T = T(\mathbf{L}, \mathbf{C})$. Note that T is a linear transformation from $\mathbf{f}$ to $\mathbf{g}$, but T depends nonlinearly on $\mathbf{L}$ and $\mathbf{C}$.

The central result of this paper is the derivation and demonstration of an algorithm that accepts as input a desired transfer matrix T_d and produces as output a 2-D LC lattice whose transfer matrix is very close to T_d. We formulate this as the following optimization problem:

$$(\mathbf{L}^*, \mathbf{C}^*) = \arg \min_{(\mathbf{L},\mathbf{C})} \|T(\mathbf{L}, \mathbf{C}) - T_d\|_F^2,$$

H. S. Bhat is with the School of Natural Sciences, University of California, Merced, Merced, CA 95343 USA email: hbhat@ucmerced.edu

B. Osting is with the Department of Applied Physics and Applied Mathematics, Columbia University, New York, NY 10027 USA email: bro2103@columbia.edu

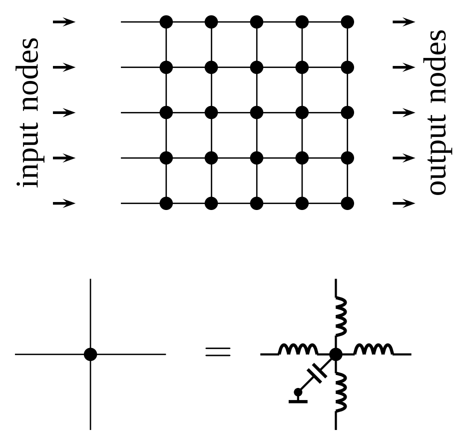

Fig. 1. (top) A graph that represents a 2-D LC lattice. (bottom) Each node represents a capacitor connected to ground. Each edge represents an inductor. The capacitances and inductances vary throughout the lattice.

where $\|\cdot\|_F$ is the Frobenius norm. We cannot expect this optimization problem to be solvable for all possible matrices T_d; however, we demonstrate that a large class of transfer matrices can be attained, with the norm difference between the true and desired transfer matrices on the order of 10^{-5}. Our approach to solving the design problem can be generalized to lattice topologies other than the one chosen here.

The general outline of our paper is as follows. In Section II, the synthesis problem is formulated as an optimization problem. The objective function makes use of the transfer matrix steady-state solution of Kirchhoff's laws on the lattice. The gradient and Hessian of the objective function are calculated analytically in Section III. In Section IV, we define design variables that reduce the dimensionality of the problem. In Section V, we present and discuss numerical solutions of the optimization problem formulated in this paper. We solve the design problem for four different transfer functions: (A) a diagonal transfer matrix, (B) a rank-one projection, (C) a low-pass filter, and (D) a power combiner/funnel. For the low-pass filter, we present results on the robustness of the optimal solution. Finally, we present two results on the ill-posedness of the synthesis problem.

A. Motivation and Context

The motivation for this work stems from a number of analog devices that operate in the 30-400 GHz range. Earlier work [2] demonstrated that an inhomogeneous 2-D LC lattice could be used as a power combiner, which was used to implement a power amplifier that generates 125mW at 85 GHz [3], more than three times the maximum reported power output for an amplifier in the same frequency range on a silicon substrate. Electrical prisms [4], filters that spatially separate the frequency content of an input signal, have been designed using 2-D LC lattices, implemented on chip, tested using 30-50 GHz inputs, and shown to have quality factors from 8 to 12. Simulations show that these filters should scale up to 200-400 GHz. Other work shows that 2-D LC lattices can be used to design a 4-bit quantizer that can process 2×10^{10} samples/sec consuming 194 mW [5], as well as a device that performs discrete Fourier transforms in space [6].

Because the 2-D LC lattice consists only of passive components, it has the desirable properties of high cut-off frequency, low latency, and high throughput, especially as compared with active-device solutions on the same substrate [2].

This paper represents a first step towards automatic synthesis of 2-D LC lattices that can be used in high-frequency analog devices. We develop a framework to study and design these lattices, potentially including all applications listed above. Of course, framing the synthesis problem in the language of optimization does not guarantee its solvability. In this paper, we give computational evidence that, for a large class of desired transfer matrices, the synthesis problem is solvable using gradient-based algorithms.

We now place our problem in the context of problems that have appeared in the literature.

Analog Circuit Design / Device Sizing. The idea of using optimization to synthesize analog circuits has been explored by many authors [7]–[12] for a variety of figures of merit. One popular approach wraps an optimization method, either gradient- or stochastic-based, around existing circuit simulation software, such as HSPICE or Spectre. There are several tools that employ this strategy, such as SPICE OPUS [13] and DELIGHT.SPICE [14], which can be used for sizing up to ≈ 100 components. There have also been numerous efforts to use genetic algorithms and neural networks for analog device synthesis—see, *e.g.*, [15] and [12, Chap 3.3.3].

Another approach is to mathematically model a circuit and then apply optimization to the model. Examples include [16], where convex programming is applied to a posynomial model of an op-amp; [17], [18], where Newton and quasi-Newton methods are applied to Kirchhoff's law models of small analog circuits; and [19], where transistor-level simulations are used to fit quadratic models that are then optimized using geometric programming. For larger problems, hierarchical methods, which build large devices from smaller ones, may be applied [8], [10], [11]; a key step is the use of device-level simulations to extract macromodels that can be used for synthesis.

Our focus in this paper on the design of 2-D LC lattices has important ramifications for the structure and size of the resulting optimization problem and leads to several differences from the works cited above.

First, the 2-D LC lattice is, by definition, a multiple-input, multiple-output (MIMO) device. A vector of inputs applied to the left boundary is transformed spatially into a vector of outputs at the right boundary. While [17], [18] do use Kirchhoff's law models and gradient-based optimization in much the same way we do, these works synthesize single-input, single-output (SISO) devices. Such devices operate in the time domain, and a typical application is pulse shaping.

One way that the difference between SISO and MIMO design manifests itself is that the optimization problem framed in this paper involves more degrees of freedom than considered in the above works. For a 2-D LC lattice of size $m \times n$, there are $N = (3m - 1)n$ unknown lattice components; note that in Section V-D, we design a 31×31 lattice where $N = 2,852$.

Second, the structure of our optimization problem allows us to fruitfully derive and apply analytical expressions for (i) the solution of the forward problem and (ii) the derivatives of the objective function. Using these analytical expressions in conjunction with quasi-Newton methods is what makes the design problem tractable, especially at large lattice sizes. Other analytical approaches for the forward problem have been explored [20]–[22] and may, in future works, be applied to the optimization problem as well.

Finally, we seek to synthesize a 2-D LC lattice from scratch, rather than improve upon an existing design, in contrast to some of the above papers and also, *e.g.*, [23]–[26].

Inverse Problems. We first mention *transmission line synthesis*: given a finite 1-D LC lattice, an input $f(t)$, and an output $g(t)$, solve for $(\mathbf{L}, \mathbf{C})$ such that when we apply $f(t)$ to one side of the 1-D LC lattice, we obtain $g(t)$ at the other side. This problem was solved 30 years ago using inverse scattering [27]–[29]—here, $f(t)$ and $g(t)$ are prescribed for all t, including both transient and steady-state responses. In contrast, for 2-D LC lattice synthesis, we assume time-harmonic inputs and consider only the steady-state output.

Two-dimensional electromagnetic inverse problems have been considered by numerous authors, *e.g.*, [30]–[33]. These problems are posed on infinite, continuous domains. Far-field scattering data is used to reconstruct unknown parameters $\varepsilon(x, y)$ and/or $\mu(x, y)$, assumed to be inhomogeneous within a compact region. Related work [34]–[36] seeks to design electromagnetic devices that either have prescribed radiative behavior in the far field, or that have optimal values of various far-field figures of merit, *e.g.*, directivity, gain, and signal-to-noise ratio. In 2-D LC lattice synthesis, the domain is discrete and finite, and the output signal is collected immediately adjacent to the scattered obstacle, a completely different regime.

Inverse problems on lattices of resistors have been extensively studied by, *e.g.*, [37], [38]. Like 2-D LC lattice synthesis, these problems are discrete inverse problems on finite domains. The goal is to reconstruct the conductivity in the interior of the lattice using measurements made using DC sources on the boundary. The resistor lattice is fundamentally different from the LC lattice: the forward problem for a resistor lattice is a discretization of the heat equation, and its steady-state solution is a smooth distribution. For 2-D LC lattices, on the other hand, the forward problem is a discretization of Maxwell's equations for spatially varying ϵ and μ [39], and the steady-state solution is a superposition of standing waves.

II. Formulation of the synthesis / design problem

The notation and formulation developed in this section is similar to that in [39], where we discuss the continuum limit of Kirchhoff's laws on a lattice.

We consider a 2-D rectangular LC lattice, as shown in Fig. 1, which we represent as an oriented, planar graph, c.f. [40, Chap. 13]. Nodes represent capacitors and edges represent inductors. The orientation of the edge represents the direction of positive current flow through the associated inductor.

In a lattice of size $m\times n$, there are mn nodes and $(2m-1)n$ edges, mn horizontal ones and $(m-1)n$ vertical ones. Let $\mathfrak{N} = \{1, 2, \ldots, mn\}$ denote the set of all nodes, and $\mathfrak{E} = \{1, 2, \ldots, (2m-1)n\}$ the set of all edges. Let $\mathbf{C}$ be a vector of size mn such that C_j is the capacitance at node j. Let $\mathbf{L}$ be a vector of size $(2m-1)n$ such that L_j is the inductance at edge j. We decompose $\mathbf{L} = [\mathbf{L}_h, \mathbf{L}_v]$ into the horizontal and vertical inductors, respectively. We denote by $V_j(t)$ the voltage across capacitor j and by $I_k(t)$ the current across inductor k at time t. By $\mathbf{V}(t)$ and $\mathbf{I}(t)$ we denote the vectors of all voltages and currents, respectively.

Of the horizontal edges, there are m boundary edges that form a subset $\Gamma \subset \mathfrak{E}$, each of which is incident upon only one node. In Fig. 1, Γ is the left-most column of horizontal edges. All other edges in the graph are incident upon two nodes. In general, an edge is an ordered pair (i_1, i_2), where $i_k \in \mathfrak{N}$. The direction of the edge is given by the ordering of these numbers, so that i_1 is the tail and i_2 is the head. For a boundary edge j that is incident only upon node i, we write $j = (\emptyset, i)$.

Let $\mathfrak{B}$ denote the $|\mathfrak{N}| \times |\mathfrak{E}| = mn \times (2m-1)n$ incidence matrix for the oriented graph that represents our circuit. Then

$$\mathfrak{B}_{ij} = \begin{cases} 1 & \text{if } j = (i', i) \text{ for some } i' \in \mathfrak{N} \cup \{\emptyset\} \\ -1 & \text{if } j = (i, i') \text{ for some } i' \in \mathfrak{N} \\ 0 & \text{otherwise.} \end{cases}$$

The matrix $\mathfrak{B}$ will be used shortly to write Kirchhoff's laws in a compact form.

In addition to the structure described already, the 2-D rectangular LC lattice also has resistors and forcing along the boundary. We represent the set of nodes connected to resistors by $\mathfrak{G} \subset \mathfrak{N}$, and let G_i be the conductance of node $i \in \mathfrak{G}$. We then extend G_i by defining $G_i \equiv 0$ for all $i \in \mathfrak{N} \setminus \mathfrak{G}$, so that $\mathbf{G} = (G_1, \ldots, G_{mn})$ is a vector in $\mathbb{R}^{|\mathfrak{N}|}$.

Let $N = |\mathfrak{N}| + |\mathfrak{E}| = (3m-1)n$. Then we define the $|\Gamma| \times N = m \times (3m-1)n$ projection matrix P_Γ by $(P_\Gamma)_{ij} = 1$ if $\Gamma_i = j$ and $(P_\Gamma)_{ij} = 0$ otherwise. Note that because $\Gamma_i \in \mathfrak{E}$, the final mn columns of P_Γ are all zero. The forcing applied at edges Γ is given by $\mathbf{W}(t) = P_\Gamma^t \mathbf{f} e^{2\pi\imath\alpha t}$, where $\mathbf{f} \in \mathbb{C}^{|\Gamma|}$.

Kirchhoff's Laws on this inductor-capacitor lattice can now be written in the following matrix-vector form:

$$\operatorname{diag}(\mathbf{L}) \frac{\mathrm{d}\mathbf{I}}{\mathrm{d}t} = -\mathfrak{B}^t \mathbf{V} + \mathbf{W} \tag{1a}$$

$$\operatorname{diag}(\mathbf{C}) \frac{\mathrm{d}\mathbf{V}}{\mathrm{d}t} = \mathfrak{B}\mathbf{I} - \operatorname{diag}(\mathbf{G})\mathbf{V} \tag{1b}$$

Define $\mathbf{z}(t) = (\mathbf{I}(t), \mathbf{V}(t))$ so for each t, $\mathbf{z}(t) \in \mathbb{C}^N$. Define

$$M(\mathbf{G}) = \begin{bmatrix} 0 & -\mathfrak{B}^t \\ \mathfrak{B} & -\operatorname{diag}(\mathbf{G}) \end{bmatrix}.$$

Then the system (1) can be written in the form

$$\operatorname{diag}(\mathbf{L}, \mathbf{C}) \dot{\mathbf{z}}(t) = M(\mathbf{G})\mathbf{z}(t) + P_\Gamma^t \mathbf{f} e^{2\pi\imath\alpha t}. \tag{2}$$

Let $\Upsilon \subset \mathfrak{G}$ denote the vector of right boundary nodes. Let P_Υ be the $|\Upsilon| \times N$ projection matrix defined by $(P_\Upsilon)_{ij} = 1$ if $\Upsilon_i = j$ and $(P_\Upsilon)_{ij} = 0$ otherwise. Note that because $\Upsilon_i \in \mathfrak{N}$, columns 1 to $|\mathfrak{E}| = (2m-1)n$ of P_Υ are all zero.

Forward Problem. Let $\mathbf{z}(t) = \mathbf{u}e^{2\pi\imath\alpha t}$. Then the forward problem is to find $\mathbf{g} = P_\Upsilon \mathbf{u}$ given $\mathbf{f}$, $\mathbf{L}$, $\mathbf{C}$, and $\mathbf{G}$. Using the Fourier transform, one can show that the solution of the forward problem is

$$\mathbf{f} \mapsto \mathbf{g} = P_\Upsilon \Big(2\pi\imath\alpha \operatorname{diag}(\mathbf{L}, \mathbf{C}) - M(\mathbf{G})\Big)^{-1} P_\Gamma^t \mathbf{f}. \tag{3}$$

Given $\operatorname{diag}(\mathbf{L}, \mathbf{C}, \mathbf{G})$, we define the *transfer matrix* to be:

$$T(\mathbf{L}, \mathbf{C}, \mathbf{G}) := P_\Upsilon \Big(2\pi\imath\alpha \operatorname{diag}(\mathbf{L}, \mathbf{C}) - M(\mathbf{G})\Big)^{-1} P_\Gamma^t. \tag{4}$$

We have formulated the circuit as an oriented graph in order to write the equations compactly and take advantage of the graph-theoretic interpretation of the incidence matrix $\mathfrak{B}$, which appears naturally in Kirchhoff's laws. Though we have formulated the problem for an $m \times n$ rectangular lattice, the beauty of the graph-theoretic framework outlined above is that it easily accommodates other lattice topologies.

Note that since (3) is invariant under the transformation

$$\alpha \mapsto \tau\alpha \quad \text{and} \quad (\mathbf{L}, \mathbf{C}) \mapsto \tau^{-1}(\mathbf{L}, \mathbf{C}), \tag{5}$$

a lattice with values $(\mathbf{L}, \mathbf{C})$ which performs a transfer function at frequency α can be rescaled by a factor of α'/α to create a lattice that performs the same function at frequency α'.

Design / Synthesis Problem. We define the admissible set

$$\begin{aligned} \mathfrak{A} := \{(\mathbf{L}, \mathbf{C}, \mathbf{G})\colon \ & \underline{L} < L_i < \overline{L} && \text{for all } i \in \mathfrak{E}, \\ & \underline{C} < C_j < \overline{C} && \text{for all } j \in \mathfrak{N}, \text{ and} \\ & \underline{G} < G_j < \overline{G} && \text{for all } j \in \mathfrak{G} \subset \mathfrak{N}\} \end{aligned}$$

where $\underline{L}$, $\overline{L}$, $\underline{C}$, $\overline{C}$, $\underline{G}$, and $\overline{G}$ are constants. Let

$$\{(\mathbf{f}^i, \mathbf{g}^i) \,|\, 1 \le i \le p\}$$

be a collection of desired input-output pairs. The design problem is: find $(\mathbf{L}, \mathbf{C}, \mathbf{G}) \in \mathfrak{A}$ such that for each i, the steady-state output $T\mathbf{f}^i$ generated by input $\mathbf{f}^i$ is equal to $\mathbf{g}^i$. We formulate this as the constrained optimization problem:

$$\min_{(\mathbf{L}, \mathbf{C}, \mathbf{G}) \in \mathfrak{A}} \quad \mathcal{J}(\mathbf{u}^i) := \frac{1}{2} \sum_{i=1}^{p} \Big\| P_\Upsilon \mathbf{u}^i - \mathbf{g}^i \Big\|^2 \tag{6a}$$

$$\text{s.t.} \quad \Big(2\pi\imath\alpha \operatorname{diag}(\mathbf{L}, \mathbf{C}) - M(\mathbf{G})\Big)\mathbf{u}^i = P_\Gamma^t \mathbf{f}^i, \quad 1 \le i \le p. \tag{6b}$$

It is convenient to set $p = m$ and choose the input basis vectors to be $(f^i)_j = \delta_{ij}$. The *desired transfer matrix* is then

$$T_d = [\mathbf{g}^1 | \mathbf{g}^2 | \cdots | \mathbf{g}^m].$$

We can then write the solution of (6b) using (4) and rewrite the optimization problem (6) in the following compact form:

$$\min_{(\mathbf{L}, \mathbf{C}, \mathbf{G}) \in \mathfrak{A}} \quad \tilde{\mathcal{J}}(\mathbf{L}, \mathbf{C}, \mathbf{G}) := \frac{1}{2} \| T(\mathbf{L}, \mathbf{C}, \mathbf{G}) - T_d \|_F^2. \tag{7}$$

As written, the objective function $\mathcal{J}(\mathbf{u}^i)$ in (6a) does not depend explicitly on $(\mathbf{L}, \mathbf{C}, \mathbf{G})$, only implicitly through the constraint (6b). We use the notation $\tilde{\mathcal{J}}(\mathbf{L}, \mathbf{C}, \mathbf{G}) = \mathcal{J}(\mathbf{u}^i(\mathbf{L}, \mathbf{C}, \mathbf{G}))$ to refer to the composition that explicitly depends on $(\mathbf{L}, \mathbf{C}, \mathbf{G})$.

We consider two different choices of boundary conditions:

(BC1) The resistive boundary $\mathfrak{G}$ consists of all nodes on the top, right, and bottom boundaries of the lattice. For each $i \in \mathfrak{G}$, we prescribe the locally impedance-matched conductance

$$G_i = \sqrt{C_i/L_j}, \tag{8}$$

where $j \in \mathfrak{E}$ is the edge incident on node i that is normal to the boundary. This impedance boundary condition can be viewed as a first-order discretization of the Silver-Müller outgoing boundary condition for Maxwell's equations, as described in [39].

(BC2) The resistive boundary $\mathfrak{G}$ consists only of Υ, *i.e.*, the nodes on the right boundary of the lattice. For each $i \in \mathfrak{G}$, we set G_i according to (8), as before. Unlike the previous case, $G_i = 0$ along top/bottom boundaries.

Slightly abusing notation, we take $\tilde{\mathcal{J}}(\mathbf{L}, \mathbf{C})$ to be the composition of $\tilde{\mathcal{J}}(\mathbf{L}, \mathbf{C}, \mathbf{G})$ with (8). We thus arrive at the following N-dimensional optimization problem:

$$\min_{(\mathbf{L},\mathbf{C})\in\mathfrak{A}} \quad \tilde{\mathcal{J}}(\mathbf{L}, \mathbf{C}) \tag{9}$$

where $\mathfrak{A}$ is also modified to reflect (8) by letting $\underline{G}_j = 0$ and $\overline{G}_j = \infty$ for all $j \in \mathfrak{G}$. Thus the only constraints in (9) are box constraints on the design variables $\mathbf{L}$ and $\mathbf{C}$.

Numerical tests show (9) is not convex, which implies that the solution to (9) is not guaranteed to be unique.

III. Computation of the Gradient and Hessian

In this section, we compute the gradient and Hessian of $\tilde{\mathcal{J}}(\epsilon)$ in preparation for quasi-Newton and Newton numerical solutions of the optimization problem (6).

A. Computation of the Gradient via the Adjoint Method

Here we set $\mathbf{s} = (\mathbf{L}, \mathbf{C})$ and $A = 2\pi\imath\alpha \operatorname{diag}(\mathbf{s}) - M$. We introduce the dual variables $\mathbf{v}^i \in \mathbb{C}^p$ and the Lagrangian

$$\mathcal{L}(\mathbf{u}^i, \mathbf{v}^i, \mathbf{s}) = \mathcal{J}(\mathbf{u}^i) + \sum_{i=1}^{p} \Re\langle \mathbf{v}^i, A\mathbf{u}^i - P_\Gamma^t \mathbf{f}^i \rangle. \tag{10}$$

The state equations (6b) are obtained by setting the derivative of (10) with respect to $\mathbf{v}^{i*}$ equal to zero. The adjoint equations are obtained by setting the derivative of (10) with respect to the state variables $\mathbf{u}^i$ equal to zero:

$$\frac{\partial \mathcal{L}}{\partial \mathbf{u}^i} = \frac{\partial \mathcal{J}}{\partial \mathbf{u}^i} + \frac{1}{2}\mathbf{v}_i^* A = 0. \tag{11}$$

Here we use

$$\frac{\partial \mathcal{J}}{\partial \mathbf{u}^i} = \frac{1}{2}(P_\Upsilon \mathbf{u}^i - \mathbf{g}^i)^* P_\Upsilon. \tag{12}$$

The decision equations are obtained by setting the derivative of (10) with respect to the design variables $\mathbf{s}$ equal to zero and recalling $\dfrac{\partial \mathcal{J}}{\partial s_k} = 0$ for all k.

$$\frac{\partial \mathcal{L}}{\partial s_k} = \sum_{i=1}^{p} \Re\left\langle \mathbf{v}^i, \frac{\partial A}{\partial s_k}\mathbf{u}^i \right\rangle = 0 \tag{13}$$

To compute $\partial A/\partial s_k$, we must compute

$$\frac{\partial \operatorname{diag}(\mathbf{s})_{ij}}{\partial s_k} = \delta_{ij}\delta_{ik} \quad \text{and} \quad \frac{\partial M}{\partial s_k} = \begin{bmatrix} 0 & 0 \\ 0 & -\dfrac{\partial G}{\partial s_k} \end{bmatrix}.$$

It is easy to show that $\partial G_{ij}/\partial s_k = 0$ unless the node k is a top, right, or bottom boundary node. There are three cases for the non-zero entries: non-corner top/bottom, non-corner right, and corners, each of which can be computed using (8).

The KKT equations consist of (6b), (11), and (13). A full space method involves the simultaneous solution of these three nonlinear equations. Alternatively, the reduced space method consists of taking $\tilde{\mathcal{J}}(\mathbf{s}) = \mathcal{J}(\mathbf{u}^i(\mathbf{s}))$. Then we have

$$\frac{\partial \tilde{\mathcal{J}}}{\partial s_k} = \Re \sum_{i=1}^{p} \left\langle \mathbf{v}^i, \frac{\partial A}{\partial s_k}\mathbf{u}^i \right\rangle, \tag{14}$$

where $\mathbf{v}^i$ and $\mathbf{u}^i$ are solutions of (6b) and (11).

B. Direct Computation of the Gradient

Here we compute

$$\begin{aligned} \frac{\partial \tilde{\mathcal{J}}}{\partial s_k} &= \frac{\partial \mathcal{J}}{\partial s_k} + \sum_{i=1}^{p} \frac{\partial \mathcal{J}}{\partial \mathbf{u}^i}\frac{\partial \mathbf{u}^i}{\partial s_k} + \frac{\partial \mathcal{J}}{\partial \mathbf{u}^{i*}}\frac{\partial \mathbf{u}^{i*}}{\partial s_k} \\ &= 2\Re \sum_{i=1}^{p} \frac{\partial \mathcal{J}}{\partial \mathbf{u}^i}\left(-A^{-1}\frac{\partial A}{\partial s_k}\mathbf{u}^i\right) \end{aligned} \tag{15}$$

where we have used

$$\frac{\partial A}{\partial s_k}\mathbf{u}^i + A\frac{\partial \mathbf{u}^i}{\partial s_k} = 0, \tag{16}$$

obtained from differentiating (6b). We now see that (14) and (15) are the same by (11). The advantage to computing $\mathbf{v}^i$ first and then computing the gradient via (14) is that only p adjoint solves are required (one for each input-output pair). Computing (15) literally (*i.e.*, computing the expression in parentheses first and then computing the vector-matrix product) would require $N \cdot p$ state solves [41].

C. Computation of the Hessian

Differentiating (14) enables us to write the Hessian

$$\begin{aligned} \frac{\partial^2 \tilde{\mathcal{J}}}{\partial s_j \partial s_k} = \Re \sum_{i=1}^{p} \mathbf{v}^{i*}\left[\frac{\partial^2 A}{\partial s_j \partial s_k}\right]\mathbf{u}^i \\ + \frac{\partial \mathbf{v}^{i*}}{\partial s_j}\left[\frac{\partial A}{\partial s_k}\right]\mathbf{u}^i + \mathbf{v}^*\left[\frac{\partial A}{\partial s_k}\right]\frac{\partial \mathbf{u}^i}{\partial s_j}. \end{aligned}$$

Differentiating the adjoint eq. (11) with respect to s_j, gives

$$\begin{aligned}\frac{\partial \mathbf{v}^{i*}}{\partial s_j} &= -\left(2\frac{\partial}{\partial s_j}\frac{\partial \mathcal{J}}{\partial \mathbf{u}^i} + \mathbf{v}^{i*}\left[\frac{\partial A}{\partial s_j}\right]\right)A^{-1}\\ &= -\left(\frac{\partial \mathbf{u}^{i*}}{\partial s_j}P_\Upsilon^t P_\Upsilon + \mathbf{v}^{i*}\left[\frac{\partial A}{\partial s_j}\right]\right)A^{-1}.\end{aligned}$$

Combining the previous two equations with (16), and defining $h_{ji} = P_\Upsilon A^{-1}\frac{\partial A}{\partial s_j}\mathbf{u}^i$, we have the Hessian

$$\begin{aligned}\frac{\partial^2 \tilde{\mathcal{J}}}{\partial s_j \partial s_k} &= \Re \sum_{i=1}^{p} h_{ji}^* h_{ki}\\ &+ \mathbf{v}^{i*}\left[\frac{\partial^2 A}{\partial s_j \partial s_k} - \frac{\partial A}{\partial s_j}A^{-1}\frac{\partial A}{\partial s_k} - \frac{\partial A}{\partial s_k}A^{-1}\frac{\partial A}{\partial s_j}\right]\mathbf{u}^i. \quad (17)\end{aligned}$$

IV. Design Variables

To reduce the size of the optimization problem (9), we introduce *design variables*, a reduced representation for $\mathbf{L}$ and $\mathbf{C}$. There are many natural choices for the design variables $\mathbf{r}$. The following choices are labeled for future reference.

(D1) If $\mathbf{L}$ and $\mathbf{C}$ are symmetric in the sense that

$$L^h_{i,j} = L^h_{m+1-i,j}, \qquad L^v_{i,j} = L^v_{m+1-i,j},$$
$$C_{i,j} = C_{m+1-i,j},$$

then the transfer matrix satisfies $T_{i,j} = T_{m+1-i,m+1-j}$. Thus, if the desired transfer matrix has this property, $\mathbf{r}$ can be chosen to enforce this symmetry on $\mathbf{L}$ and $\mathbf{C}$. This reduces the dimension of the design variable space by a factor of approximately two.

(D2) The vectors $\mathbf{L}_h$ and $\mathbf{L}_v$ can be chosen as a discretization of a single continuous function $\mu(\mathbf{x})$ as in [39]. This imposes a compatibility condition on $\mathbf{L}_h$ and $\mathbf{L}_v$, reducing the dimension of the design space by approximately three. Specifically, we let $\boldsymbol{\mu}$ be a $m+1 \times n+1$ matrix and set

$$L^h_{ij} = \frac{1}{2}\left(\mu_{ij} + \mu_{i+1,j}\right),\ 1 \le i \le m,\ 1 \le j \le n \quad \text{(18a)}$$
$$L^v_{ij} = \frac{1}{2}\left(\mu_{ij} + \mu_{i,j+1}\right),\ 2 \le i \le m,\ 1 \le j \le n. \quad \text{(18b)}$$

The design variables then consist of $\mathbf{C}$ and $\boldsymbol{\mu}$.

(D3) Restricting to lattices with $\mathbf{L} = 1$ reduces the dimension of the design space by a factor of three. This is analogous to considering media with constant permeability [39].

(D4) Combining the ideas in (D1) and (D3), we take $\mathbf{L} = 1$ and force C to have symmetry. This reduces the design variable space by a factor of six.

(D5) The vectors $\mathbf{L}$ and $\mathbf{C}$ can also be represented in terms of a truncated basis, such as the Fourier, wavelet, or block bases, but we do not pursue this here.

For a (BC1) lattice, energy leaks out of the top/bottom boundaries, so the total energy collected at the output is less than the input energy. Since we are primarily interested in the shape of the output $g(y)$, we include an extra design variable δ in the objective function (9), replacing T_d by δT_d. For all design variable choices, we let $r_1 = \delta$.

Let $\mathbf{s} = \mathbf{s}(\mathbf{r})$ denote the dependence of $\mathbf{s}$ on a set of design variables $\mathbf{r}$. Then the gradient and Hessian can be computed

$$g \equiv \nabla_\mathbf{r} \tilde{\mathcal{J}}(\mathbf{s}(\mathbf{r})) = \mathbf{s_r} \nabla_\mathbf{s} \tilde{\mathcal{J}}$$
$$H \equiv \nabla_\mathbf{r}\nabla_\mathbf{r} \tilde{\mathcal{J}}(\mathbf{s}(\mathbf{r})) = \mathbf{s_r}\nabla_\mathbf{s}\nabla_\mathbf{s}\tilde{\mathcal{J}}\mathbf{s}^t_\mathbf{r},$$

where $\mathbf{s_r}$ denotes the Jacobian and $\nabla_\mathbf{s}\tilde{\mathcal{J}}$ and $\nabla_\mathbf{s}\nabla_\mathbf{s}\tilde{\mathcal{J}}$ were computed in (14) and (17) respectively.

Once the design variables are chosen, the optimization problem (9) can be written

$$\min_{\mathbf{r} \in \mathfrak{A}_r} \quad \tilde{\mathcal{J}}(\mathbf{r}) := \frac{1}{2}\|T(\mathbf{r}) - r_1 T_d\|_F^2 \qquad (20)$$

where $\mathfrak{A}_r$ is an admissible set for the design variables $\mathbf{r}$,

$$\mathfrak{A}_r := \{\mathbf{r}: \quad \underline{r} \le r_j \le \overline{r} \quad \text{for all } j\}.$$

V. Computational Results

In Sections V-A through V-D, we apply gradient-based optimization tools [42] to solve the lattice synthesis problem (20) for four desired transfer matrices. In Section V-A, we also compare the performance of several different optimization methods. In Sec. V-C we compare the two choices of boundary conditions given in Sec. II. In all other sections, we use (BC1). In Section V-E, we discuss the sensitivity of the transfer matrix of an inductor-capacitor lattice to small perturbations in $\mathbf{L}$ or $\mathbf{C}$. Finally, in Sections V-F and V-G, we study numerically the well-posedness of the synthesis problem.

A. Diagonal Transfer Matrix

In this section, we define the desired transfer matrix to be the diagonal matrix $T_d = \mathrm{diag}(\mathbf{t})$. For a lattice with m rows, let $j_c = (m+1)/2$ and $t_j = \exp(-2(j-j_c)^2)$, $j = 1, \ldots, m$. We set $\alpha = .08$ and choose (D1) design variables with lower and upper bounds 0.05 and 5.

We now solve the synthesis problem (20) for an $m \times m$ lattice for $m = 8$ ($N = 184$) and $m = 16$ ($N = 752$) using several different numerical methods. For each m and numerical method used, in Fig. 2, we plot both iteration number and wall time vs. the objective function value. In what follows, we describe the methods compared in Fig. 2. All computations were done using Matlab 7.11 on a 2.4 GHz Intel Core 2 Duo desktop computer with 2GB of RAM. In each case, the convergence criteria was set using the Matlab options: `MaxIter` $= 2000$, `TolX` $= 10^{-14}$, and `TolFun` $= 10^{-13}$. In all examples here and below, the optimization method is initialized with constant design variables, $\mathbf{r}$. We compare Matlab's `fmincon` implementation of the following nonlinear constrained optimization algorithms:

(SQ) `sqp`: The sequential quadratic programming (SQP) approach is to approximate (20) by a quadratic minimization problem at each iteration. This quadratic form involves the Hessian of the objective function, which is approximated using the BFGS method [42, Ch. 18].

(AS) `active-set`: The active set method solves a sequence of unconstrained optimization problems. The optimization variables do not necessarily satisfy the bounds at each iteration.

(IP) `interior-point`: This line-search based quasi-Newton method uses the BFGS method to update the approximate Hessian at each iteration. The constraints are enforced using a logarithmic barrier function.

(TR) `trust-region-reflective`: We use this subspace trust-region method with `large-scale` = `off`.

From Fig. 2, we conclude that all tested methods are able to find solutions with low objective values. The other methods perform approximately the same in both iteration count and wall time. The interior point method (IP) performs best; however, the solution obtained tends to be less smooth than that obtained via the other methods. In what follows, we primarily use the (AS) method. In addition to the four methods described above, we also tried Newton's method, but found that the cost of computing the Hessian (17) was prohibitively large for lattice sizes of interest.

Let us return to the design problem for the diagonal transfer matrix T_d. The optimal solution $(\mathbf{L}^*, \mathbf{C}^*)$ for $m = 16$ obtained using (SQ) is plotted in Fig. 3 and has objective value $J = 7.3 \times 10^{-5}$. The method terminated when the maximum number of iterations, `MaxIter` $= 2000$, was reached.

For this transfer function and *all* transfer functions considered in the subsequent sections, the design variable $r_1 = \delta$ attains the lower bound constraint of $\underline{r}_1 = .6$. This indicates it is easier to synthesize energy-dissipative lattices.

B. Waveguide Filter / Rank-One Projection

In this section, we define

$$T_d = \begin{pmatrix} \ddots & \vdots & \vdots & \vdots & \vdots & \iddots \\ \cdots & 0 & 0 & 0 & 0 & \cdots \\ \cdots & 0 & 1 & 1 & 0 & \cdots \\ \cdots & 0 & 1 & 1 & 0 & \cdots \\ \cdots & 0 & 0 & 0 & 0 & \cdots \\ \iddots & \vdots & \vdots & \vdots & \vdots & \ddots \end{pmatrix},$$

the discrete analogue of a waveguide transfer function $f \mapsto \langle \psi, f \rangle \psi$, where ψ is a desired bound state.

With $\alpha = .32$, we use (D1) design variables with lower and upper bounds given by 0.05 and 50. For a 24×24 lattice, we use the active set method (AS) to obtain the optimal solution $(\mathbf{L}^*, \mathbf{C}^*)$ plotted in Fig. 4 with objective value $J = 6 \times 10^{-6}$. The method terminated after 547 iterations because the predicted change in the objective function was less than `TolFun` $= 10^{-13}$.

The optimal solution, plotted in Fig. 4, has horizontal inductors $\mathbf{L}^h$ and capacitors $\mathbf{C}$ which take large values in a strip from the center inputs to the center outputs. Outside of this strip, the C matrix has periodic structure arranged to impede an incoming wave. The fact that we can recognize structure in the solution to an optimization problem in $\mathbb{R}^{1704}$ is remarkable, and suggests rigidity in the synthesis problem.

C. A Low-Pass Filter / Smoothing Convolution

In [39], we used separation of variables to obtain the exact solution for the continuous analogue of the forward problem (3) for a homogeneous lattice. We concluded that a homogenous lattice strongly damps oscillatory input, which

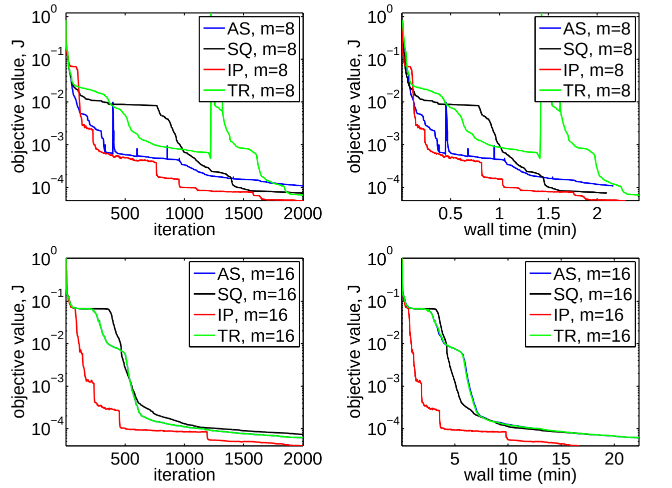

Fig. 2. We plot (left) iteration number vs. objective function value and (right) wall time vs. objective function value for the solution of (20) on an $m \times m$ lattice for $m = 8$ (top) and $m = 16$ (bottom) and various optimization methods (see Sec. V-A for method abbreviation definitions).

suggests that this type of lattice is well-suited for performing low-pass filtering functions. We investigate this intuition here by constructing a circuit that behaves as a low-pass filter.

For an 8×6 lattice, we define the transfer matrix:

$$T_d = \frac{1}{44} \begin{pmatrix} 2 & 1 & 0 & 0 \\ 4 & 2 & 1 & 0 \\ 8 & 4 & 2 & 1 \\ 4 & 8 & 4 & 2 \\ 2 & 4 & 8 & 4 \\ 1 & 2 & 4 & 8 \\ 0 & 1 & 2 & 4 \\ 0 & 0 & 1 & 2 \end{pmatrix}. \tag{21}$$

The matrix T_d can be obtained by removing the first two and last two columns from an 8×8 Toeplitz matrix. We also remove the first and last two columns of the transfer matrix T in (20). With $\alpha = 0.16$ and (D1) design variables with lower and upper bounds given by $.05$ and 50, we use the active set method (AS) for each of the boundary conditions given in Sec. II. For (BC1), the final objective function value is $J = 6.24 \times 10^{-7}$ and for (BC2), the final objective value is $J = 2.98 \times 10^{-5}$. In both cases, the method terminated because the predicted change in the objective function was less than `TolFun` $= 10^{-13}$. In Fig. 5, we plot the optimal solution $(\mathbf{L}^*, \mathbf{C}^*)$ for both choices of boundary conditions.

D. Power Combiner / Funnel

Motivated by the power combiner introduced in [2], [3], we consider the transfer matrix that maps all inputs to the center output. The desired transfer matrix T_d of size $m \times m$ (where $m = 2j + 1$ is odd) consists of a matrix where row $j + 1$ has a 1 in each column, and all other rows are identically zero.

We set $\alpha = 0.08$ and choose (D2) design variables. The upper and lower bounds were $.05$ and 20. In Fig. 6, we plot the optimal solution $(\mathbf{L}^*, \mathbf{C}^*)$ for the synthesis problem attained using the active set method (AS). The solution is plotted for $m \times m$ lattices where $m = 11$, 21, and 31 with respective objective function values 2×10^{-5}, 3×10^{-5}, and 3×10^{-5}.

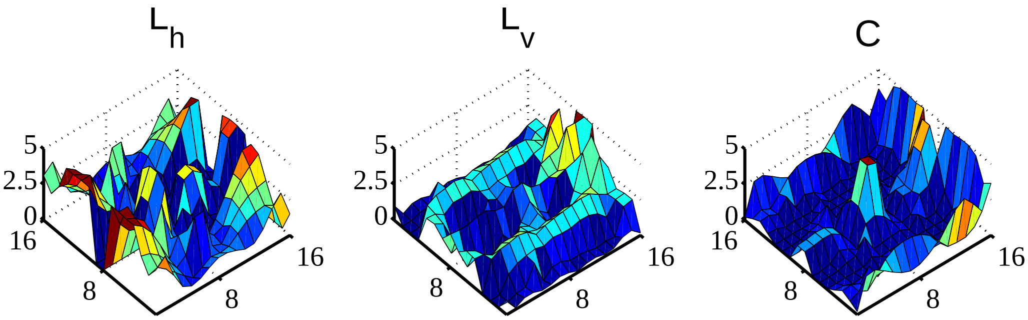

Fig. 3. The $(\mathbf{L}, \mathbf{C})$ matrices for the 16×16 diagonal transfer lattice found in Section V-A with objective value $J = 7.3 \times 10^{-5}$.

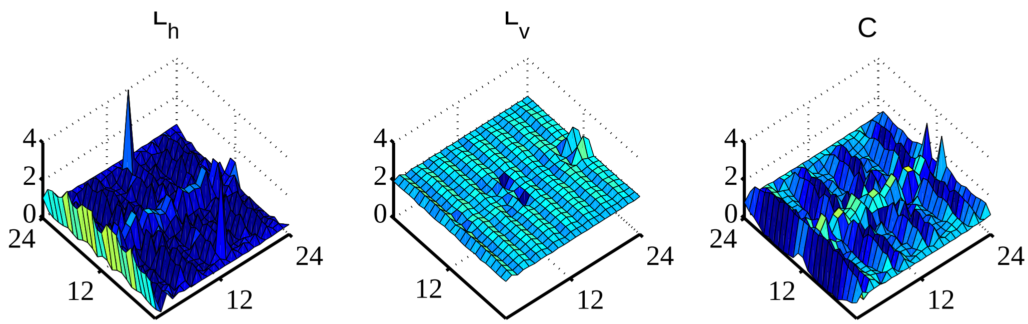

Fig. 4. The $(\mathbf{L}, \mathbf{C})$ matrices for the 24×24 waveguide in Section V-B with objective value $J = 6 \times 10^{-6}$.

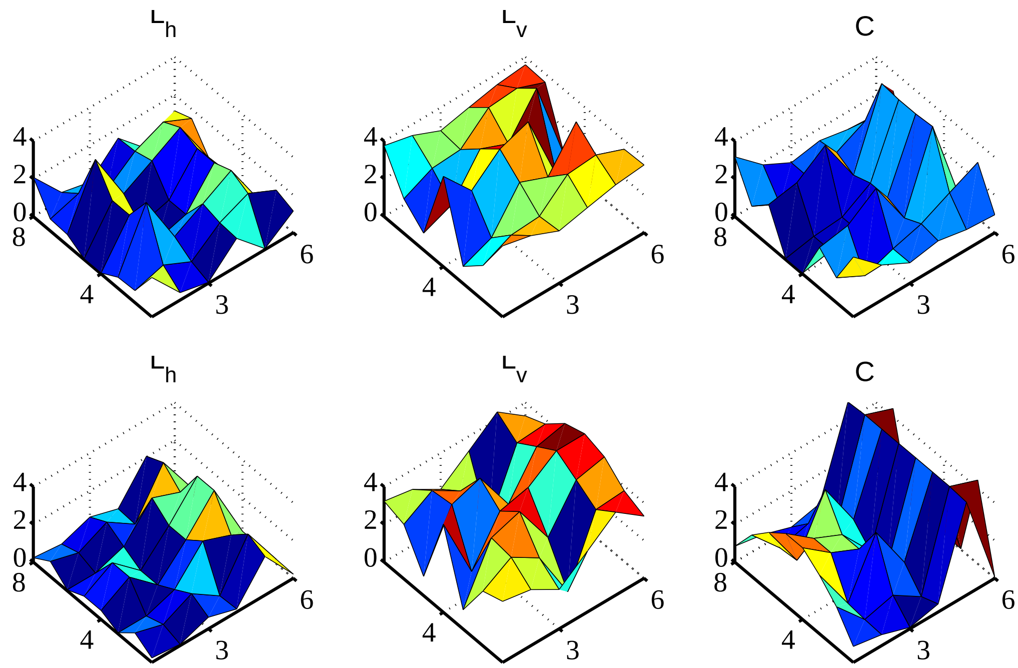

Fig. 5. The $(\mathbf{L}, \mathbf{C})$ matrices for the low-pass filter in Section V-C for the 8×6 lattice for boundary conditions as described by (BC1) in the top panel and (BC2) in the lower panel with resp. objective values $J = 6.24 \times 10^{-7}$ and $J = 2.98 \times 10^{-5}$.

In each case, the method terminated because the maximum number of iterations, $\texttt{MaxIter} = 3000$, was reached.

E. Robustness / Sensitivity of Optimal Devices

In this section, we consider the sensitivity of optimal devices to small changes in $(\mathbf{L}, \mathbf{C}, \mathbf{G})$. We begin with a proposition that is proved in Appendix A.

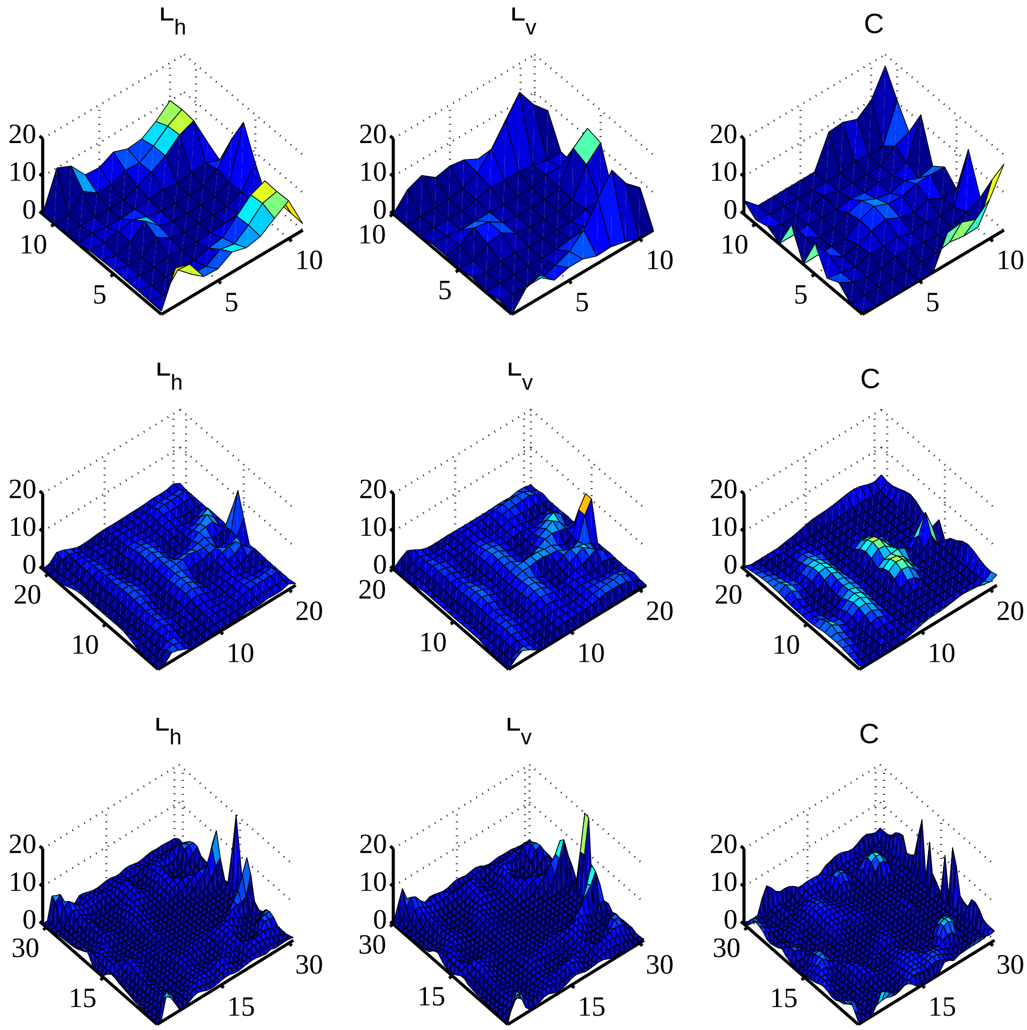

Fig. 6. The $(\mathbf{L}, \mathbf{C})$ surfaces for the funnel in Sec. V-D for the $m \times m$ lattice for $m = 11$, 21, 31 with objective values 2×10^{-5}, 3×10^{-5}, and 3×10^{-5}.

Proposition 1. *Let $T_j = P_\Upsilon A_j^{-1} P_\Gamma^t$, $j = 1, 2$ be the transfer matrices for two different circuits with capacitances, inductances, and conductances given by $(\mathbf{C}_j, \mathbf{L}_j, \mathbf{G}_j)$, where*

$$A_j := 2\pi\imath\alpha \operatorname{diag}(\mathbf{L}_j, \mathbf{C}_j) - M(\mathbf{G}_j).$$

Assume $\rho := \|A_1^{-1}(A_2 - A_1)\|_2 < 1$, and define $\gamma = 1/\sigma_1(A_1)$ where $\sigma_1(A_1) > 0$ is the smallest singular value of A_1. Then

$$\|T_1 - T_2\|_F \leq \frac{mN\gamma^2}{1-\rho}\Big[2\pi\alpha\left(\|\mathbf{L}_2 - \mathbf{L}_1\|_2 + \|\mathbf{C}_2 - \mathbf{C}_1\|_2\right) + \|\mathbf{G}_2 - \mathbf{G}_1\|_2\Big].$$

The upshot of this proposition is that if a circuit is perturbed by modifying $(\mathbf{L}, \mathbf{C}, \mathbf{G})$, then the change in the transfer matrix for the circuit is bounded by the size of the perturbation. However, the bounding constant could be large and increases with increasing circuit size.

We conduct a numerical experiment to further investigate this dependence for the low-pass filtering device introduced in Section V-C. Let $(\mathbf{L}^*, \mathbf{C}^*)$ denote the 8×6 device with (BC1) boundary conditions plotted in Fig. 5(top panel) that minimizes $\mathcal{J}$ for the desired transfer matrix in (21) with objective value $\mathcal{J}(\mathbf{L}^*, \mathbf{C}^*) = 6.24 \times 10^{-7}$. We now evaluate $\mathcal{J}$ for a distribution of perturbations to $(\mathbf{L}^*, \mathbf{C}^*)$. Specifically, we consider multiplicative noise and evaluate $\mathcal{J}(\mathbf{L}.\mathbf{u}, \mathbf{C}.\mathbf{v})$, where $\mathbf{a}.\mathbf{b}$ denotes entry-wise multiplication of the vectors $\mathbf{a}$ and $\mathbf{b}$, and $(\mathbf{u}, \mathbf{v})$ have entries which are normally distributed with mean 1 and standard deviation 0.02. We interpret a structure $(\mathbf{L}.\mathbf{u}, \mathbf{C}.\mathbf{v})$ to be a low-pass filtering device manufactured with 2% tolerance. In Fig. 7, we plot a histogram of the objective function value evaluated on a sample size of $100,000$ drawn from this distribution. The 10th, 50th and 90th quantiles are 1.8×10^{-3}, 6.9×10^{-3}, and 3.9×10^{-2}.

We might also consider the sensitivity of optimal devices to small changes in α. However, since (6) is invariant under the transformation in (5), perturbing α is equivalent to choosing a multiplicative perturbation $(\mathbf{u}, \mathbf{v})$ from a skewed distribution.

F. Known Lattice Recovery / Inverse Crime Study

In the preceding sections, our goal was to obtain useful circuits. Here and in the next section, we conduct numerical experiments to quantify the ill-posedness of the problem.

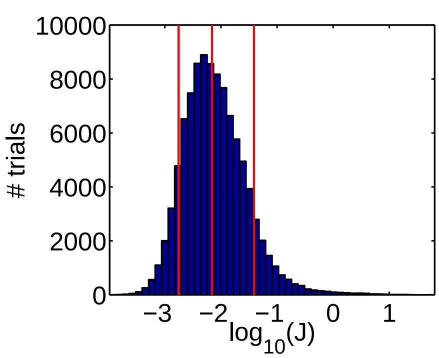

Fig. 7. A histogram of the objective function evaluated for $100,000$ low-pass filters (see Fig. 5) with 2% normally-distributed, multiplicative noise. The vertical lines indicate the 10th, 50th and 90th quantiles. See Sec. V-E.

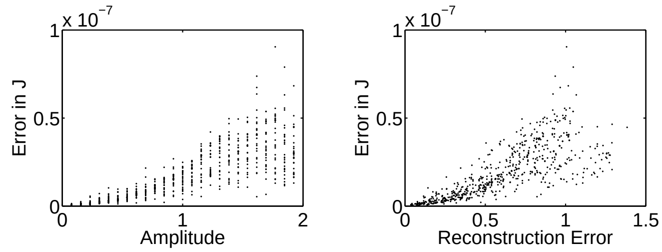

Fig. 8. Objective function value $\mathcal{J}(\mathbf{L}^*,\mathbf{C}^*)$ versus ρ (left panel) and versus $\|(\mathbf{L}^*,\mathbf{C}^*)-(\mathbf{L}^0,\mathbf{C}^0)\|_\infty$ (right panel) for 750 runs, all on 8×8 lattices. See Section V-F.

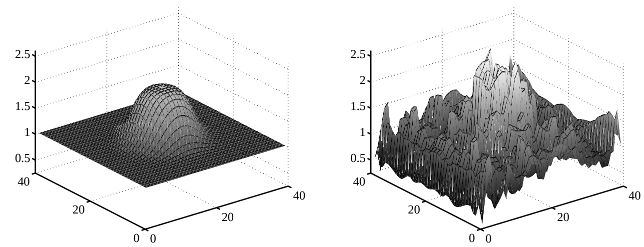

Fig. 9. A plot of the capacitance matrices $\mathbf{C}_{40}$ (left) and $\overline{\mathbf{C}}_{40}$ (right) as defined in Section V-G.

In this first numerical experiment, we commit a so-called "inverse crime." We take $p = m$ and generate a transfer matrix T_d by solving the forward problem for *known* values of $(\mathbf{L}^0,\mathbf{C}^0)$. We then set aside $(\mathbf{L}^0,\mathbf{C}^0)$ and solve the design problem for the transfer matrix T_d, giving us a computed solution $(\mathbf{L}^*,\mathbf{C}^*)$.

This is refered to as an "inverse crime" since the model of the forward problem used to generate the transfer matrix is precisely the same model assumed in the solution of the design problem. For these transfer matrices, we happen to know that there is a point—namely $(\mathbf{L}^0,\mathbf{C}^0)$—where the objective function is zero. We can then measure how well our algorithm does by comparing $\mathcal{J}(\mathbf{L}^*,\mathbf{C}^*)$ with zero. We can also characterize the solution space by checking how $\mathcal{J}(\mathbf{L}^*,\mathbf{C}^*)$ depends on the known solution $(\mathbf{L}^0,\mathbf{C}^0)$.

Let us describe how we generate a random matrix $\mathbf{C}^0$. We fix integer parameters $\nu > 0$ and σ as well as real parameters ρ_{min} and ρ_{max}. We choose two random vectors of Fourier sine coefficients $\mathbf{k}^x$ and $\mathbf{k}^y$, both of size $\nu\times 1$. The j-th entry $k_j^{(\cdot)}$ is sampled from a $U(0,1)$ distribution and then multiplied by $j^{-\sigma}$. We sample $P(x,y) = \sum_{i=1}^{\nu}\sum_{j=1}^{\nu} k_i^x k_j^y \sin(ix)\sin(jy)$ to create an $m\times n$ matrix $\mathbf{C}^0$ that is then scaled and translated so its max/min values are, respectively, ρ_{max} and ρ_{min}.

For $\mathbf{L}^h$ and $\mathbf{L}^v$, we follow (18) after generating an $(m+1)\times(n+1)$ matrix $\boldsymbol{\mu}$ by sampling $P(x,y)$. We scale and translate the matrices $\mathbf{L}^h$ and $\mathbf{L}^\mathbf{v}$ so their max/min values are, respectively, ρ_{max} and ρ_{min}. In all cases, sampling of $P(x,y)$ is performed on a regular grid in the square $[0,2\pi]^2$.

Using the above approach for generating random pairs $(\mathbf{L}^0,\mathbf{C}^0)$, we solved the design problem 750 times on an 8×8 lattice. We used the active set method (AS) with $\texttt{TolX} = 10^{-14}$, $\texttt{TolFun} = 10^{-13}$, and (D2) design variables with lower and upper bounds of $.05$ and 50. For all 750 runs, the code terminated because the magnitude of the directional derivative in the search direction was less than $2\,\texttt{TolFun}$.

We stepped ν from 0 to 5 and σ from 1 to 5. We stepped ρ through 25 equispaced values in the interior of $(0,2)$, and set $\rho_{\text{max}} = 1+\rho/2$, $\rho_{\text{min}} = 1-\rho/2$.

In the left panel of Fig. 8, we plot the objective function value $\mathcal{J}(\mathbf{L}^*,\mathbf{C}^*)$ versus amplitude ρ for all 750 runs. The plot shows that the code performed very well across all runs, with the maximum value of $\mathcal{J}(\mathbf{L}^*,\mathbf{C}^*)$ less than 10^{-7}. The plot also reflects a correlation coefficient of 0.82, which indicates that the larger the amplitude of spatial oscillations in $\mathbf{L}^0$ and $\mathbf{C}^0$, the poorer the quality of the local optimum reached.

In the right panel of Fig. 8, we plot the objective function value $\mathcal{J}(\mathbf{L}^*,\mathbf{C}^*)$ versus reconstruction error $\|(\mathbf{L}^*,\mathbf{C}^*)-(\mathbf{L}^0,\mathbf{C}^0)\|_\infty$ for all 750 runs. The plot reflects that, as we move further away from the global minimum $(\mathbf{L}^*,\mathbf{C}^*)$, we are still able to achieve transfer matrices that are very close to what is desired. However, the correlation coefficient of 0.80 indicates a small degradation in the quality of the local optima as a function of distance from a global optimum.

G. Lattice Refinement and Coarsening

For a lattice with homogeneous $(\mathbf{L},\mathbf{C})$ the Nyquist principle states that $\alpha\sqrt{LC} < \sqrt{2}/\pi$. In [21], we found that Kirchhoff's laws (3) behave like their continuum limit if $\alpha\sqrt{LC} < 1/(2\pi)$, which is roughly one-third of the Nyquist frequency. In [39] we showed that the continuum limit is precisely the system of equations for the (H_1,H_2,E) polarized mode for Maxwell's equations in a planar medium. Thus we expect that for α sufficiently small, even if $(\mathbf{L},\mathbf{C})$ is inhomogeneous, one may increase the size of the lattice and rescale $(\mathbf{L},\mathbf{C})$ so that both problems are a discretization of the same continuum problem.

In this section, we use this principle to provide quantitative estimates on the ill-posedness of the synthesis problem. Throughout, we set $\mathbf{L}=1$ and $\alpha = 1$.

On a 40×40 lattice, we set $C_{ij} = 1 + \operatorname{sech}^2\gamma\left((i-20.5)^2+(j-20.5)^2\right)$ for $\gamma = 25/39^2$. Using this $\mathbf{C}_{40}$, we solve (3) for the transfer matrix T_{40}.

We then average 2×2 subblocks of both T_{40} and $\mathbf{C}_{40}$ to obtain a transfer function T_{20} and capacitances $\mathbf{C}_{20}$ on a $20\times$

20 lattice. The vector $\mathbf{C}_{20}$ is divided by 4 based on the finite volume derivation in [39]. The synthesis problem with desired transfer function T_{20} is then initialized using $\mathbf{C}_{20}$ and solved using (D4) decision variables. We denote this solution $\tilde{\mathbf{C}}_{20}$ and note that the objective function value is $\mathcal{J} = 3.7 \times 10^{-3}$.

We now refine $\tilde{\mathbf{C}}_{20}$ to a 40×40 lattice by repeating 2×2 blocks of $\tilde{\mathbf{C}}_{20}$. We denote these capacitances by $\tilde{\mathbf{C}}_{40}$. The synthesis problem with transfer function T_{40} is initialized using $\tilde{\mathbf{C}}_{40}$ and solved to obtain $\overline{\mathbf{C}}_{40}$. Both surfaces are plotted in Fig. 9. The final value of the objective function is 9.5×10^{-8} and $\|\overline{\mathbf{C}}_{40} - \mathbf{C}_{40}\|_F = 11.1$. Thus, $\mathbf{C}_{40}$ and $\overline{\mathbf{C}}_{40}$ are far apart in the Frobenius norm but achieve almost the same transfer function. Although the problem is ill-posed and the solution obtained is different than $\mathbf{C}_{40}$, we emphasize that we view $\overline{\mathbf{C}}_{40}$ as a excellent solution to the synthesis problem since it achieves a phenomenally low objective function value.

In inverse problems, one applies regularization methods to enforce *a priori* known information such as smoothness. Similarly, in the design problem considered here, where the "data" (*i.e.*, desired transfer matrix) is known perfectly, one could apply regularization methods to force $\mathbf{L}$ and $\mathbf{C}$ to have desired properties. We do not pursue this direction here.

VI. Conclusion / Discussion

We have formulated the two-dimensional transmission lattice synthesis problem as an optimization problem, the solution of which yields inductor-capacitor lattices that can be fabricated for custom/novel applications in analog signal processing and filtering. For several chosen transfer functions, we have demonstrated that gradient-based optimization methods can be used to obtain excellent solutions to the synthesis problem.

In other contexts, the ideas presented in this paper are familiar: one can engineer the permittivity ε and permeability μ of a medium to control the propagation of EM waves [43], [44], and in quantum mechanics, one may engineer a potential to have desired scattering properties [45]. As the frequency of analog circuits marches into the THz range, it is increasingly important that the circuit model be related, both qualitatively and quantitatively, to Maxwell's equations. Ultimately, if one is interested in designing a microwave frequency device, one performs a direct numerical simulation of Maxwell's equations to confirm that the circuit model accurately predicts the device's behavior. Based on our findings in [39], these connections can be made more precise. Kirchhoff's laws for the 2-D LC lattice (1) can be viewed as a finite volume discretization of Maxwell's equations for a planar, inhomogeneous medium. For large circuits with smoothly varying $(\mathbf{C}, \mathbf{L})$, this discretization is accurate, and one can interpret the present work as a discretize-then-optimize approach to solving the (ε, μ) synthesis problem for Maxwell's equations. This is the subject of forthcoming work.

Appendix A
Proof of the proposition in Section V-E

The matrix identity $A^{-1} - B^{-1} = A^{-1}(B - A)B^{-1}$ gives

$$T_1 - T_2 = P_\Upsilon A_1^{-1}(A_2 - A_1)A_2^{-1}P_\Gamma^t.$$

Taking the Frobenius norm of both sides and using the the sub-multiplicative property of the Frobenius norm we obtain

$$\|T_1 - T_2\|_F \le \|P_\Upsilon A_1^{-1}\|_F \|A_2 - A_1\|_F \|A_2^{-1}P_\Gamma^t\|_F. \quad (22)$$

We treat the 3 pieces on the right hand side of (22) in turn. First note $\|P_\Upsilon\|_F = |\Upsilon|^{1/2} = \sqrt{m}$ and $\|P_\Gamma\|_F = |\Gamma|^{1/2} = \sqrt{m}$.

1. We compute

$$\|P_\Upsilon A_1^{-1}\|_F \le \|P_\Upsilon\|_F \|A_1^{-1}\|_F \le \sqrt{m}\sqrt{N}\|A_1^{-1}\|_2 = \sqrt{mN}\gamma.$$

Here we used the norm relation: $\|A\|_F \le \sqrt{r}\|A\|_2$ where r is the rank of A and $\|A_1^{-1}\|_2 = \sigma_N(A_1^{-1}) = 1/\sigma_1(A_1) = \gamma$.

2. We compute

$$\begin{aligned}\|A_2 - A_1\|_F &\le 2\pi\alpha\|\operatorname{diag}(\mathbf{L}_2, \mathbf{C}_2) - \operatorname{diag}(\mathbf{L}_1, \mathbf{C}_1)\|_F \\ &\quad + \|M(\mathbf{G}_2) - M(\mathbf{G}_1))\|_F \\ &= 2\pi\alpha\left(\|\mathbf{L}_2 - \mathbf{L}_1\|_2 + \|\mathbf{C}_2 - \mathbf{C}_1\|_2\right) \\ &\quad + \|\mathbf{G}_2 - \mathbf{G}_1\|_2.\end{aligned}$$

3. As above, we compute

$$\|A_2^{-1}P_\Gamma^t\|_F \le \|A_2^{-1}\|_F \|P_\Gamma^t\|_F \le \sqrt{mN}\|A_2^{-1}\|_2.$$

Our goal now is to estimate $\|A_2^{-1}\|_2$ in terms of γ. We compute

$$\begin{aligned}\|A_2^{-1}\|_2 &= \|\left[A_1\left(\mathrm{Id} + A_1^{-1}(A_2 - A_1)\right)\right]^{-1}\|_2 \\ &= \|\left(\mathrm{Id} + A_1^{-1}(A_2 - A_1)\right)^{-1} A_1^{-1}\|_2 \\ &\le \gamma\|\left(\mathrm{Id} + A_1^{-1}(A_2 - A_1)\right)^{-1}\|_2\end{aligned}$$

Note that $\left(\mathrm{Id} + A_1^{-1}(A_2 - A_1)\right)^{-1}$ exists by the assumption $\rho < 1$. Summing the Neumann series for this expression gives

$$\begin{aligned}\|\left(\mathrm{Id} + A_1^{-1}(A_2 - A_1)\right)^{-1}\|_2 &\le \sum_{j=0}^{\infty}\|A_1^{-1}(A_2 - A_1)\|_2^j \\ &= \sum_{j=0}^{\infty}\rho^j = \frac{1}{1-\rho}.\end{aligned}$$

Putting these 3 pieces together yields the desired result.

Acknowledgment

This material is based upon work supported by the National Science Foundation (NSF) under Grants DMS09-13048 and DMS06-02235, EMSW21-RTG: Numerical Mathematics for Scientific Computing. Any opinions, findings, and conclusions or recommendations expressed in this material are those of the author(s) and do not necessarily reflect the views of the NSF. The authors would like to thank the NSF Institute for Pure and Applied Mathematics (IPAM) for its hospitality.

References

[1] L. Brillouin, *Wave Propagation in Periodic Structures. Electric Filters and Crystal Lattices*, ser. International Series in Pure and Applied Physics. McGraw-Hill, 1946.

[2] E. Afshari, H. S. Bhat, A. Hajimiri, and J. E. Marsden, "Extremely wideband signal shaping using one- and two-dimensional nonuniform nonlinear transmission lines," *J. Appl. Phys.*, vol. 99, no. 5, p. 054901, 2006.

[3] E. Afshari, H. S. Bhat, X. Li, and A. Hajimiri, "Electrical Funnel: a New Signal Combining Method," in *Proceedings of the IEEE International Solid-State Circuits Conference (ISSCC'06)*, San Francisco, CA, Feb. 2006, pp. 206–208.

[4] O. Momeni and E. Afshari, “Electrical Prism: A High Quality Factor Filter for Millimeter-Wave and Terahertz Frequencies,” *IEEE Trans. Microw. Theory Tech.*, vol. 57, no. 11, pp. 2790–2799, 2009.
[5] Y. M. Tousi and E. Afshari, “2-D Electrical Interferometer: A Novel High-Speed Quantizer,” *IEEE Trans. Microw. Theory Tech.*, vol. 58, no. 10, pp. 2549–2561, 2010.
[6] E. Afshari, H. S. Bhat, and A. Hajimiri, “Ultrafast analog Fourier transform using two-dimensional LC lattice,” *IEEE Trans. Circuits Syst. I, Reg. Papers*, vol. 55, no. 8, pp. 2332–2343, 2008.
[7] G. G. E. Gielen and R. A. Rutenbar, “Computer-aided design of analog and mixed-signal integrated circuits,” *Proc. IEEE*, vol. 88, no. 12, pp. 1825–1852, 2000.
[8] R. A. Rutenbar, G. G. E. Gielen, and J. Roychowdhury, “Hierarchical modeling, optimization, and synthesis for system-level analog and RF designs,” *Proc. IEEE*, vol. 95, no. 3, pp. 640–669, 2007.
[9] E. S. J. Martens and G. G. E. Gielen, *High-Level Modeling and Synthesis of Analog Integrated Systems*. Springer, 2008.
[10] S. H. M. Ali, “System level performance and yield optimisation for analogue integrated circuits,” Ph.D. dissertation, University of Southampton, 2009.
[11] J. Zou, “Hierarchical optimization of large-scale analog/mixed-signal circuits based-on pareto-optimal fronts,” Ph.D. dissertation, Technische Universität München, 2009.
[12] R. Hägglund, “An optimization-based approach to efficient design of analog circuits,” Ph.D. dissertation, Linköping University Institute of Technology, 2006.
[13] J. Olenšek, A. Bűrmen, J. Puhan, and T. Tuma, “Automated analog electronic circuits sizing,” in *Differential Evolution*, A. Qing, Ed. Wiley, 2009, pp. 353–367.
[14] W. Nye, D. C. Riley, A. Sangiovanni-Vincentelli, and A. L. Tits, “DELIGHT.SPICE: an optimization-based system for the design of integrated circuits,” *IEEE Trans. Comput.-Aided Design*, vol. 7, no. 4, pp. 501–519, 1988.
[15] J. R. Koza, F. H. Bennett, D. Andre, M. A. Keane, and F. Dunlap, “Automated synthesis of analog electrical circuits by means of genetic programming,” *IEEE Trans. Evol. Comput.*, vol. 1, no. 2, pp. 109–128, 1997.
[16] M. D. Hershenson, S. P. Boyd, and T. H. Lee, “Optimal design of a CMOS op-amp via geometric programming,” *IEEE Trans. Comput.-Aided Design Integr. Circuits Syst.*, vol. 20, no. 1, pp. 1–21, 2001.
[17] V. L. Chechurin, N. V. Korovkin, and M. Hayakawa, *Inverse Problems in Electric Circuits and Electromagnetics*. Springer, 2007.
[18] O. Wing, *Classical Circuit Theory*. Springer, 2008.
[19] X. Li, P. Gopalakrishnan, Y. Xu, and L. T. Pileggi, “Robust analog/RF circuit design with projection-based performance modeling,” *IEEE Trans. Comput.-Aided Design Integr. Circuits Syst.*, vol. 26, no. 1, pp. 2–15, 2007.
[20] B. Osting and H. S. Bhat, “Dispersive diffraction in a two-dimensional hexagonal transmission lattice,” in *Proceedings of the International Symposium on Antennas and Propagation (ISAP ’08)*, Taipei, Taiwan, Oct. 2008.
[21] H. S. Bhat and B. Osting, “Diffraction on the two-dimensional square lattice,” *SIAM J. Appl. Math.*, vol. 70, no. 5, pp. 1389–1406, 2009.
[22] ——, “Discrete diffraction in two-dimensional transmission line metamaterials,” *Microwave and Optical Technology Letters*, vol. 52, no. 3, pp. 721–725, 2010.
[23] G. D. Hachtel, R. K. Brayton, and F. G. Gustavson, “The sparse tableau approach to network analysis and design,” *IEEE Trans. Circuit Theory*, vol. 18, no. 1, pp. 101–113, 1973.
[24] R. K. Brayton, S. W. Director, G. D. Hachtel, and L. M. Vidigal, “A new algorithm for statistical circuit design based on quasi-Newton methods and function splitting,” *IEEE Trans. Circuits Syst.*, vol. 26, no. 9, pp. 784–794, 1979.
[25] R. K. Brayton, G. D. Hachtel, and A. L. Sangiovanni-Vincentelli, “A survey of optimization techniques for integrated-circuit design,” *Proc. IEEE*, vol. 69, no. 10, pp. 1334–1362, 1981.
[26] J. Bandler and S. Chen, “Circuit optimization: the state of the art,” *IEEE Trans. Microw. Theory Tech.*, vol. 36, no. 2, pp. 424–443, 1988.
[27] R. E. Caflisch, “An inverse problem for Toeplitz matrices and the synthesis of discrete transmission lines,” *Linear Algebra and its Applications*, vol. 38, pp. 207–225, 1981.
[28] B. W. Dickinson, “An inverse problem for Toeplitz matrices,” *Linear Algebra and its Applications*, vol. 59, pp. 79–83, 1984.
[29] A. M. Bruckstein and T. Kailath, “Inverse scattering for discrete transmission-line models,” *SIAM Review*, vol. 29, no. 3, pp. 359–389, 1987.
[30] D. Colton and R. Kress, *Inverse Acoustic and Elecromagnetic Scattering Theory, Second Edition*. Springer, 1998.
[31] J. L. Frolik and A. E. Yagle, “A discrete-time formulation for the variable wave speed scattering problem in two dimensions,” *Inverse Problems*, vol. 12, pp. 909–924, 1996.
[32] ——, “Forward and inverse scattering for discrete layered lossy and absorbing media,” *IEEE Trans. Circuits Syst. II, Analog Digit. Signal*, vol. 44, pp. 710–722, 1997.
[33] A. E. Yagle and J. L. Frolik, “On the feasibility of impulse reflection response data for the two-dimensional inverse scattering problem,” *IEEE Trans. Antennas Propag.*, vol. 44, pp. 1551–1564, 1996.
[34] T. S. Angell and A. Kirsch, *Optimization Methods in Electromagnetic Radiation*, ser. Springer Monographs in Mathematics. Springer, 2004.
[35] C. A. Balanis, *Antenna Theory: Analysis and Design*. Wiley, 2005.
[36] W. L. Stutzman and G. A. Thiele, *Antenna Theory and Design*. Wiley, 1998.
[37] E. B. Curtis and J. A. Morrow, *Inverse Problems for Electrical Networks*, ser. Series on applied mathematics. World Scientific, 2000.
[38] L. Borcea, V. Druskin, A. V. Mamonov, and F. G. Vasquez, “Pyramidal resistor networks for electrical impedance tomography with partial boundary measurements,” *Inverse Problems*, vol. 26, no. 10, p. 105009, 2010.
[39] H. S. Bhat and B. Osting, “Kirchhoff’s laws as a finite volume method for a planar Maxwell system,” *IEEE Trans. Antennas Propag.*, 2011, accepted and in press.
[40] L. R. Foulds, *Graph Theory Applications*. Springer, 1992.
[41] G. Strang, *Computational Science and Engineering*. Wellesley-Cambridge Press, 2007.
[42] J. Nocedal and S. Wright, *Numerical Optimization*, 2nd ed. Springer, 2006.
[43] M. Burger, S. Osher, and E. Yablonovitch, “Inverse problem techniques for the design of photonic crystals,” *IEICE Trans. Electron.*, vol. 87, pp. 258–265, 2004.
[44] J. D. Joannopoulos, S. G. Johnson, J. N. Winn, and R. D. Meade, *Photonic Crystals: Molding the Flow of Light*, 2nd ed. Princeton, NJ: Princeton University Press, 2008.
[45] B. Osting and M. I. Weinstein, “Emergence of periodic structure from maximizing the lifetime of a bound state coupled to radiation,” *SIAM Multiscale Model Simul.*, 2011, in press.